

Motion Planning for Multi-Link Robots by Implicit Configuration-Space Tiling*

Oren Salzman[†], Kiril Solovey[†] and Dan Halperin[†]

Abstract— We study the problem of motion-planning for free-flying multi-link robots and develop a sampling-based algorithm that is specifically tailored for the task. Our approach exploits the fact that the set of configurations for which the robot is *self-collision free* is independent of the obstacles or of the exact placement of the robot. This allows for decoupling between costly self-collision checks on the one hand, which we do off-line (and can even be stored permanently on the robot’s controller), and collision with obstacles on the other hand, which we compute in the query phase. In particular, given a specific robot type our algorithm precomputes a *tiling roadmap*, which efficiently and implicitly encodes the self-collision free (sub-)space over the entire configuration space, where the latter can be infinite for that matter. To answer a query, which consists of a start position, a target region, and a *workspace environment*, we traverse the tiling roadmap while only testing for collisions with obstacles. Our algorithm suggests more flexibility than the prevailing paradigm in which a precomputed roadmap depends both on the robot and on the scenario at hand. We demonstrate the effectiveness of our approach on open and closed-chain multi-link robots, where in some settings our algorithm is more than fifty times faster than commonly used, as well as state-of-the-art solutions.

I. INTRODUCTION

Motion planning is a fundamental problem in robotics. In its most basic form, it is concerned with moving a robot from start to target while avoiding collisions with obstacles. Initial efforts in motion planning have focused on designing complete analytical algorithms (see, e.g., [1]), which aim to construct an explicit representation of the free space—the set of collision-free configurations. However, with the realization that such approaches are computationally intractable [2], even for relatively-simple settings, the interest of the Robotics community has gradually shifted to *sampling-based* techniques for motion planning [3], [4]. Such techniques attempt to capture the connectivity of the free space by random sampling, and are conceptually simple, easy to implement, and remarkably efficient in practical settings. As such, they are widely used in practice. Another key advantage of these techniques is that they are typically described in general terms and can often be applied to a wide range of robots and scenarios. However, this also has its downsides. Due to the limited reliance of sampling-based algorithms on the specific structure of the problem at hand,

they tend to overlook unique aspects of the problem, which might be exploited to increase the efficiency of such methods. For instance, a more careful analysis of the specific problem may result in a reduced reliance on collision detection, which is often considered to be the bottleneck component in sampling-based algorithms.

In this paper we study the problem of planning the motion of a *multi-link* robot, which consists of multiple rigid links connected by a set of joints (see Fig. 1). We assume that the robot is *free flying*, i.e., none of its joints are anchored to a specific point in the workspace. We describe a novel algorithm which exploits the unique structure of the problem. Our work is based on the simple observation that the set of configurations for which the robot is not in *self collision* is independent of the obstacles or on the exact placement of the robot. This allows to eliminate costly self-collision checks in the query stage, and to carry them out during the preprocessing stage. The novelty comes from the fact that preprocessing needs to be carried out once for a given type of robot. This is in contrast to prevalent state-of-the-art techniques, such as PRM* [5], where the preprocessed structure can only be applied to a particular scenario and robot type. In some situations, self-collision checks can be as costly as obstacle-collision checks—particularly in cases where the robot consists of many links or when the links form a closed chain. Moreover, for robots of the latter type, computing local paths is particularly costly as the set of collision-free configurations lie on a low-dimensional manifold in the configuration space.

At the heart of our approach is an implicit representation of the *tiling roadmap*, which efficiently represents the space of configurations that are self-collision free. In particular, it is completely independent of the scenarios in which it can be employed. Once a query is given in the form of a scenario—a description of the workspace obstacles, a start configuration and a target region, the tiling roadmap is traversed using the recently-introduced dRRT algorithm [6].

While our current work deals with free-flying multi-link robots, we hope that it will pave the way to the development of similar techniques for various types of robots. This may have immediate practical implications: when developing a robot for mass production, a preprocessed structure, similar to the tiling roadmap, would be embedded directly to the hardware of the robot. This has the potential to reduce costly self-collision checks when dealing with complex robots.

The rest of the paper is organized as follows: We start by reviewing related work in Section II, and continue in Section III with an overview of our technique and some

[†] Oren Salzman, Kiril Solovey and Dan Halperin are with the Blavatnik School of Computer Science, Tel-Aviv University, Israel. Email: [orenzalz, kirilsol, danha]@post.tau.ac.il

* This work has been supported in part by the Israel Science Foundation (grant no. 825/15), by the German-Israeli Foundation (grant no. 1150-82.6/2011), and by the Hermann Minkowski–Minerva Center for Geometry at Tel Aviv University. Kiril Solovey is also supported by the Clore Israel Foundation.

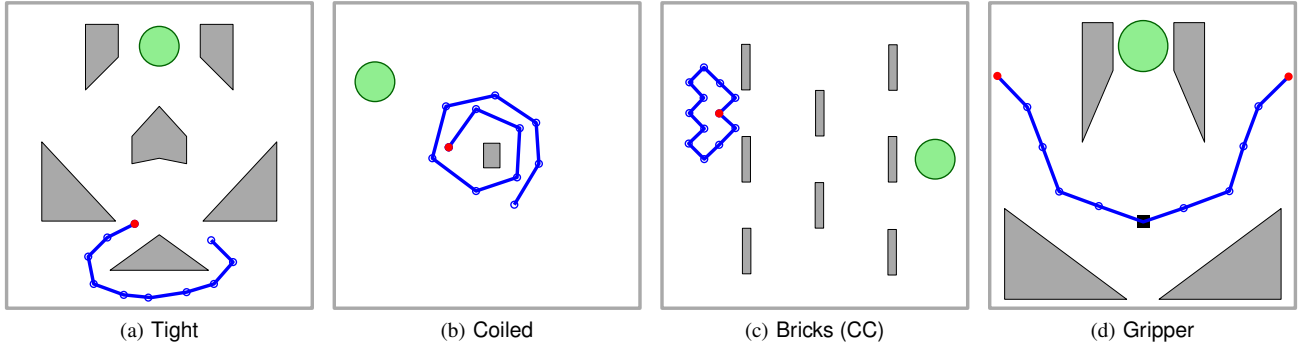


Fig. 1. Test scenarios. Robot links and anchor points are depicted in solid blue lines and blue circles respectively. The head of the robot (red) needs to move to the target region (green circle) while avoiding the obstacles (gray polygons) and self intersection. In (a) and (b) the robot consists of an open link chain, whereas in (c) the robot is a closed loop. In (d) the robot’s middle joint (black square) is permanently anchored to a specific point and both endpoints need to reach the target region

preliminary definitions. In Section IV we formally describe the tiling roadmap and in Section V describe how it should be used in order to answer motion-planning queries. We discuss the properties of the tiling roadmap in Section VI and present simulations evaluating our algorithm in Section VII. Finally, Section VIII discusses the limitations of our work and presents possible future work.

II. RELATED WORK

A common approach to plan the motion of multi-link robots is by sampling-based algorithms [3], [4]. While sampling-based planners such as PRM [7] or RRT [8] may be used for some types of multi-link robots, they are not suited for planning when the robot is constrained [9]. Thus, the recent years have seen many works attempting to sample valid configurations and to compute local paths for a variety of multi-link robots differing in the dimension of the workspace, the type of joints and the constraints on the system [9]–[16]. Additionally, there have been application-specific collision-detection algorithms for multi-link robots [17]–[20] as collision-detection is a key ingredient in the implementation of sampling-based motion-planning algorithms.

For protein chains, which are typically modelled as high-dimensional tree-shaped multi-link robots, sampling-based approaches have been used together with an energy function which guides the search in space (see, e.g., [21]–[24]). Additional applications of motion planning for multi-link robots are reconfigurable robots [25], [26] and digital actor [27]. For an overview of motion planning and additional applications see [4].

Specifically relevant to our work is the recently-introduced notion of reachable volumes [28]–[30]. The reachable volume of a multi-link system is the set of points that the end effector of the system can reach. The authors show how to compute the reachable volume and present a method for generating self-collision free configurations using reachable volumes. This method is applicable to open and closed-chain robots, tree-like robots, and robots that include both loops and open chains. Pan et al. [31] introduced a motion-planning

algorithm for articulated models such as multi-link robots, which is integrated in an RRT-like framework.

Our work shares similarities with the work by Han and Amato [11], who studied closed chain system and introduced the kinematics-based probabilistic-roadmap (KBPRM) planner. This planner constructs a local PRM roadmap that ignores the obstacles and only considers the robot’s kinematics. Then, copies of the roadmap are placed in the full configuration space and connections are made between the copies. Our work builds on several of the ideas of KBPRM. Specifically, we also exploit the fact that self-collision free configurations can be generated while avoiding obstacles and copies of these configurations may be placed together with connections in the configuration space. The main difference from our work is that the resulting roadmap of KBPRM depends on a given workspace environment. Another difference is that they need to apply rigid-body local planning when attempting to connect copies of the preprocessed local roadmap. In contrast, the implicitly-defined tiling roadmap defined in our work already encodes these precomputed self-collision free local plans. Our work also bears some resemblance to LazyPRM [32], which constructs a PRM roadmap, but entirely delays collision detection to the query stage.

Sampling-based algorithms are not the only tool used to address the problem at hand. There have been attempts to study the structure of the configuration space of multi-link robots (see, e.g., [33], [34]) or to explicitly construct it (see, e.g., [35]–[37]). Space-decomposition techniques were used to approximate the structure of the configuration space [38]–[40] and efficient graph-search algorithms were used to search in a configuration space that was discretized using a grid [41].

III. ALGORITHM OVERVIEW AND TERMINOLOGY

The tiling roadmap \mathcal{G} is an implicitly-represented infinite graph that efficiently encodes the space of self-collision free configurations of a given robot. The structure of \mathcal{G} depends only on the type of the given robot, and is completely independent of the workspace scenario in which it can be

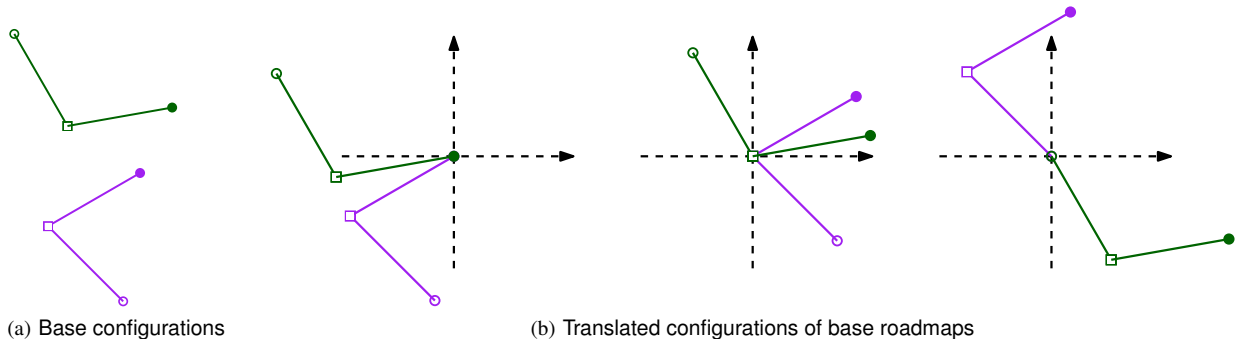


Fig. 2. Visualization of base roadmaps for a two-link planar robot. (a) Two base configurations depicted in green and purple. Notice that each anchor point is depicted differently: by a circle, a square, or a disc. (b) The three base roadmaps induced by these two base configurations.

used. Every edge of \mathcal{G} represents a motion in which one of the endpoints of the robot’s links remains fixed in space. We refer to all such endpoints as *anchor points*¹. A motion path induced by \mathcal{G} consists of a sequence of moves in which the robot alternates between the fixed anchor points in order to make progress. Given a query, which consists of a start configuration, a target region, and a workspace environment, the tiling roadmap \mathcal{G} is traversed using the dRRT [6] pathfinding algorithm (see Section V). When a configuration or an edge is considered by the pathfinding algorithm, it is only checked for collisions with the obstacles.

We now proceed with a set of definitions that will be used in the rest of the paper. Let R be a multi-link robot moving in some workspace $\mathcal{W} \subseteq \mathbb{R}^d$ (where $d \in \{2, 3\}$) cluttered with obstacles. The robot R consists of rigid links and joints connecting them. For simplicity of the exposition of the method, we focus here on robots that are “snake-like”, i.e., each anchor point connects at most two rotating rigid links and there are no loops. Thus, we assume that our robot consists of $m - 1$ rigid links and m anchor points. We stress that the technique remains correct for any other type of a free-flying multi-link robot (see experiments in Section VII). While a configuration of such a robot is usually represented by the position $p \in \mathcal{W}$ of its reference point and the angles of the joints, it will be simpler to describe our technique while representing a configuration by a collection of m points in \mathbb{R}^d , which describe the coordinates of the anchor points. Thus, we define the configuration space of the robot to be $\mathcal{C} := \{(p_1, \dots, p_m) \mid p_i \in \mathbb{R}^d\}$, such that the lengths of the links are fixed. Given an index $1 \leq j \leq m$ and a point $q \in \mathbb{R}^d$ we denote by $\mathcal{C}_j(q) := \{(p_1, \dots, p_m) \mid p_j = q, \forall i \neq j p_i \in \mathbb{R}^d\}$, the set of configurations in which the j ’th anchor point is q .

We denote the *obstacle-collision free space* by $\mathcal{F}^O \subset \mathcal{C}$. This is the set of configurations in which the robot does not collide with any obstacle. In addition, we denote the *self-collision free space* by $\mathcal{F}^S \subset \mathcal{C}$, which is the set of configurations in which no two links of the robot intersect².

¹The anchor points are not to be confused with the robot’s joints. A snake-like robot with $m - 1$ links has $m - 2$ joints but m anchor points.

²We consider a configuration to be in self collision if (i) a pair of links that do not share a joint intersect, or (ii) two consecutive links overlap.

Finally, we set $\mathcal{F} := \mathcal{F}^O \cap \mathcal{F}^S$ and refer to this set as the *free space*. In a similar fashion we define these sets for the case where the j ’th anchor point of the robot is fixed at $q \in \mathbb{R}^d$, i.e., $\mathcal{F}_j^O(q), \mathcal{F}_j^S(q), \mathcal{F}_j(q) \subset \mathcal{C}_j(q)$.

Given a configuration $C = (c_1, \dots, c_m)$ and a point $p \in \mathbb{R}^d$, let $C + p$ denote the configuration $(c_1 + p, \dots, c_m + p)$. Namely, $C + p$ is the configuration obtained by computing a vector sum of each anchor point with the vector p . We say that $C + p$ is the configuration C *translated* by p . Additionally, for a configuration C , as defined above, and an index $1 \leq j \leq m$, let $j(C) := c_j$. Namely, $j(C)$ denotes the location of the j ’th anchor point of configuration C . Finally, let $\mathbf{0}$ denote the origin of \mathbb{R}^d .

IV. TILING ROADMAPS

In this section we formally define the *tiling roadmap* \mathcal{G} , which approximates the self-collision free space \mathcal{F}^S . We first describe a basic ingredient of the tiling roadmap called *base roadmaps*. We then explain the role of base roadmaps in the construction of \mathcal{G} .

A. Base roadmaps for the anchored robot

Let $\mathbb{C}^{\text{base}} := \{C_1, \dots, C_n\} \subset \mathcal{F}^S$ be a collection of n self-collision free configurations called *base configurations*, which were uniformly and randomly sampled³. As the name suggests, the vertices of \mathcal{G} will be based upon the configurations in \mathbb{C}^{base} . In particular, every vertex of \mathcal{G} is some translation of a configuration from \mathbb{C}^{base} . Conversely, for every $C \in \mathbb{C}^{\text{base}}$ there exist infinitely many points $S = \{s_1, s_2, \dots\} \subset \mathbb{R}^d$, such that for every $s \in S$ the configuration $s + C$ is a vertex of \mathcal{G} .

In the next step, we use the configurations in \mathbb{C}^{base} to generate m roadmaps—one for each anchor point, where the j th roadmap represents a collection of configurations, and paths between them, in which the robot’s j th anchor point is fixed at the origin. More formally, the j th roadmap is embedded in $\mathcal{F}_j^S(\mathbf{0})$. For each configuration $C_i \in \mathbb{C}^{\text{base}}$, and every $1 \leq j \leq m$, we consider the configuration $C_{j,i} :=$

³In this work we only consider uniform sampling for the generation of base configurations. However, we do not exclude the possibility that more sophisticated sampling scheme will lead to better performance of the framework.

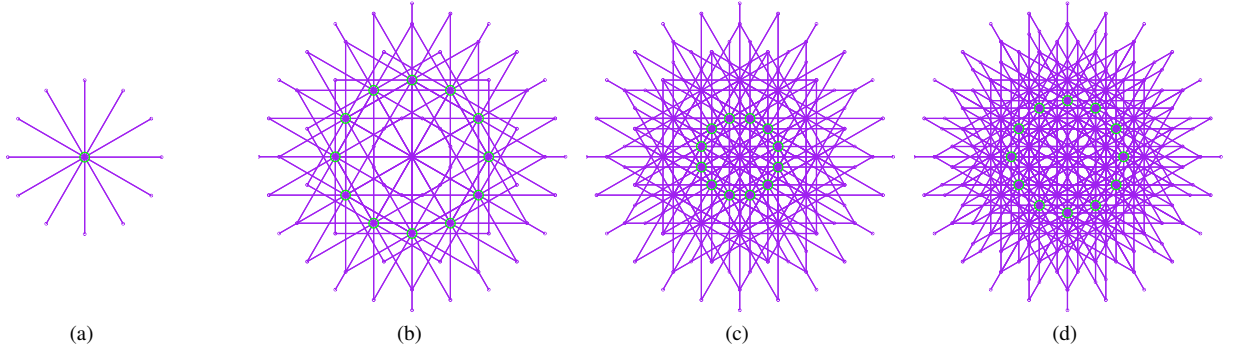


Fig. 3. The tiling roadmap for a toy example which consists of a robot with a single link. (a) Base roadmap for a single-link robot with 12 base configurations chosen at fixed intervals of $\frac{\pi}{6}$. (b)-(d) Iteratively placing the base roadmap on endpoints of the link that are closest to the origin (the current placements are highlighted by green circles).

$C_i - j(C_i)$ which represents the configuration C_i translated by $-j(C_i)$. Clearly, the j th anchor point of $C_{j,i}$ coincides with the origin. Now, set $\mathbb{C}_j^{\text{base}} := \{C_{j,1}, \dots, C_{j,n}\}$ and note that $\mathbb{C}_j^{\text{base}} \subset \mathcal{F}_j^S(\mathbf{0})$. See Fig. 2.

For every index j we construct the *base roadmap* $G_j(\mathbf{0}) = (V_j(\mathbf{0}), E_j(\mathbf{0}))$, where $V_j(\mathbf{0}) = \mathbb{C}_j^{\text{base}}$, which can be viewed as a PRM roadmap in $\mathcal{F}_j^S(\mathbf{0})$ constructed over the samples $V_j(\mathbf{0})$. We compute for each anchored configuration $C_{j,i} \in \mathbb{C}_j^{\text{base}}$ a set of k nearest neighbors⁴ from $\mathbb{C}_j^{\text{base}}$. We add an edge $E_j(\mathbf{0})$ between $C_{j,i}$ and every neighbor if the respective local path connecting the two configurations is in $\mathcal{F}_j^S(\mathbf{0})$.

B. Definition of the tiling roadmap

So far we have explicitly constructed m base roadmaps $G_1(\mathbf{0}), \dots, G_m(\mathbf{0})$, where $G_j(\mathbf{0}) \subset \mathcal{F}_j^S(\mathbf{0})$. We now show that a configuration that is a vertex in one base roadmap, can also be viewed as a vertex in the $m - 1$ remaining base roadmaps, after they undergo a certain translation (a different translation for each base roadmaps). This yields the *tiling roadmap* \mathcal{G} , in which various translations of the base roadmaps are stitched together to form a covering of \mathcal{F}^S .

Given a point $p \in \mathbb{R}^d$ we use the notation $G_j(p) = (V_j(p), E_j(p))$ to represent the roadmap $G_j(\mathbf{0})$ translated by p . We have the following observation, which follows from the construction of the base roadmaps.

Observation 1: Let C be a vertex of $G_j(\mathbf{0})$ for some j . Then C is also a vertex of $G_{j'}(j'(C))$ for any $j' \neq j$. Similarly, if C is a vertex of $G_j(p)$ for some point $p \in \mathbb{R}^d$, then it is also a vertex of $G_{j'}(p + j'(C))$.

This observation implies that a robot placed in a configuration C of $G_j(\mathbf{0})$ is not restricted to $\mathcal{F}_j(\mathbf{0})$. In particular, by viewing C as a vertex of $G_{j'}(p + j'(C))$, it can perform moves in $\mathcal{F}_{j'}(p + j'(C))$. This argument can be applied recursively, and implicitly defines the tiling roadmap $\mathcal{G} = (\mathcal{V}, \mathcal{E})$.

We can now proceed to describe the structure of \mathcal{G} in a recursive manner. Initially, \mathcal{G} contains the vertices of the base roadmaps $G_1(\mathbf{0}), \dots, G_m(\mathbf{0})$, and the corresponding edges.

⁴To compute a set of nearest neighbors, one needs to define a metric over the space. We discuss this issue in Section VII.

For every vertex C of \mathcal{G} , and every index j , the neighbors of C in $G_j(j(C))$ are added to \mathcal{G} , as well as the respective edges. To visualize the recursive definition of the tiling roadmap we examine the simple (self-collision free) case of a robot with a single link that was preprocessed with $n = 12$ base configurations. Assume that for all base configurations, the link's endpoint is fixed at the origin and the angle of the link with the x -axis is chosen at fixed intervals of $\frac{\pi}{6}$ (see Fig. 3a). To avoid cluttering the figure, we only visualize part of the recursive construction: We place a copy of this base roadmap on each of the endpoints of the link (Fig. 3b) and iteratively repeat this process for all endpoints around the origin (Fig. 3c-3d). Even for this simple example with only 12 base configurations we obtain a highly dense tiling of \mathcal{F}^S .

V. PATH PLANNING USING TILING ROADMAPS

Recall that the tiling roadmap \mathcal{G} represents the self-collision free space \mathcal{F}^S of a given robot. We describe how \mathcal{G} is used to find a solution, i.e., a path for the robot in the fully-free space \mathcal{F} , given a query that consists of a start configuration $S \in \mathcal{F}$, a target region $T \subseteq \mathcal{F}$, and a workspace environment \mathcal{W} . The solution is found by (i) adding the start configuration S to each base roadmap (together with local paths in this roadmap) and (ii) attempting to find a collision-free path from S to T using \mathcal{G} . To connect S to each base roadmap we do the following. Let $S_j := S - j(S)$ for $1 \leq j \leq m$. For every j we connect S_j to $G_j(\mathbf{0})$ by selecting a collection of nearest neighbors in $G_j(\mathbf{0})$ and applying a *local planner* which produces paths in $\mathcal{F}_j^S(\mathbf{0})$. By definition, S is a vertex of \mathcal{G} . It remains to find a path in \mathcal{G} from S to some other vertex $C \in \mathcal{V}$ such that $C \in T$ using a graph-search algorithm. Note that during the search each encountered vertex or edge of \mathcal{G} should be tested for collision with the obstacles described by \mathcal{W} . Also note that the vertices and edges are self-collision free by the definition of \mathcal{G} .

To search for a path using the tiling roadmap, one may consider employing standard pathfinding algorithms on graphs such as A* [42]. However, when the graph is dense, and the problem lacks a good heuristic function to guide the search, A* (and its many variants) resort to a BFS-like search

Algorithm 1 dRRT

```

1: loop
2:    $q_{\text{rnd}} \leftarrow \text{RANDOM\_SAMPLE}()$ 
3:    $q_{\text{near}} \leftarrow \text{NEAREST\_NEIGHBOR}(\mathcal{T}, q_{\text{rnd}})$ 
4:    $q_{\text{new}} \leftarrow \text{DIRECTION\_ORACLE}(q_{\text{near}}, q_{\text{rnd}})$ 
5:   if  $q_{\text{new}} \notin \mathcal{T}$  and  $\text{VALID}(q_{\text{near}}, q_{\text{new}})$  then
6:      $\mathcal{T}.\text{add\_vertex}(q_{\text{new}})$ 
7:      $\mathcal{T}.\text{add\_edge}(q_{\text{near}}, q_{\text{new}})$ 
8:   if  $q_{\text{new}} \in T$  then
9:     return  $\text{RETRIEVE\_PATH}(\mathcal{T}, s, T)$ 

```

which is prohibitively costly in terms of running time and memory consumption. This is backed-up by our experimental work in which A* was unable to make sufficient progress on \mathcal{G} .

Instead, our motion-planning algorithm integrates the implicitly-represented tiling roadmap \mathcal{G} with a highly-efficient pathfinding technique called discrete-RRT [6] (dRRT). We will refer to our framework as TR-dRRT, where “TR” stands for “tiling roadmap”. dRRT (Algorithm 1) is an adaptation of the RRT algorithm for the purpose of exploring discrete, geometrically-embedded graphs.

Similarly to its continuous counterpart, dRRT samples a random configuration q_{rnd} (Alg. 1, line 2), which is not necessarily a vertex of \mathcal{G} . Then, it finds the nearest neighbor q_{near} of q_{rnd} in the explored portion of \mathcal{G} (line 3), which is the tree \mathcal{T} . The difference lies in line 4. Whereas RRT usually expands the tree from q_{near} towards q_{rnd} by generating a path that linearly interpolates between the two configurations of \mathcal{G} , dRRT uses a “direction oracle” which returns a vertex q_{new} such that there is an edge from q_{near} to q_{new} in \mathcal{G} . Moreover, it is guaranteed that the direction $\overrightarrow{q_{\text{near}}q_{\text{new}}}$ is closest to the direction $\overrightarrow{q_{\text{near}}q_{\text{rnd}}}$ among all the edges of \mathcal{G} incident to q_{near} . In the next step this edge is checked for obstacle collision (line 5). If it is collision free, it is added to \mathcal{T} . See a visualization in Fig. 4.

Specifically in TR-dRRT, the direction oracle is implemented in a brute-force manner by going over all the neighbors of q_{near} in \mathcal{G} and comparing their directions. This set of neighbors is extracted as follows: Recall that for every base roadmap G_j , there exists a translation p_j such that q_{near} is a vertex of $G_j(p_j)$. We take all the neighbors q_{near} in $G_j(p_j)$, for every j .

A desirable feature of a sampling-based algorithm is that it maintains *probabilistic completeness*. Namely, as the running time of the algorithm increases, the probability that a solution is found (assuming one exists) approaches one. Indeed, the dRRT algorithm is probabilistically complete (see [6]). We believe that, under mild assumptions, one can show that the TR-dRRT framework is probabilistically complete as well. We discuss this issue in the following section.

VI. PROPERTIES OF THE TILING ROADMAP

We discuss some theoretical properties of the tiling roadmap. We begin by stating that the tiling roadmap covers

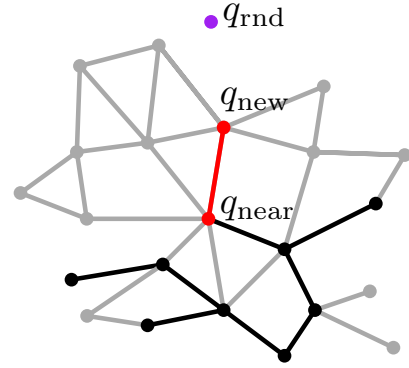


Fig. 4. dRRT algorithm. The tiling roadmap \mathcal{G} (gray vertices and edges) is traversed via subtree \mathcal{T} (explored vertices and edges depicted in black). Extension is performed by sampling a random configuration q_{rnd} (purple) and locating its nearest explored neighbor q_{near} in \mathcal{T} . The direction oracle returns a neighbor q_{new} of q_{near} , which is in the direction of q_{rnd} (red). If the edge connecting the two configurations is obstacle collision free, q_{new} is added to the explored tree. Figure adapted from [6].

the collision-free space and providing a proof sketch. Specifically, we show that for every self-collision free configuration $C_S \in \mathcal{F}^S$ there exist another configuration $C \in \mathcal{V}$ such that C_S and C are arbitrarily close as the number of samples tends to infinity. We then provide a discussion on the additional steps required to show that our method is probabilistic complete.

A. Coverage

Intuitively, as the number of base configurations grows, the tiling roadmap \mathcal{G} increases its *coverage* of \mathcal{F}^S . For simplicity, we consider a *planar* snake-like robot whose configuration space is represented by $\mathbb{R}^2 \times \mathcal{S}^1 \times \dots \times \mathcal{S}^1$. We use the term “head” to refer to the first anchor point, namely, the first endpoint of the first link, and denote by L the length of the first link. We will use the standard representation of configurations in such a configuration space. Namely, we will consider a configuration as a pair (p, Θ) , where $p = (x, y) \in \mathbb{R}^2$ is the location of the head of the robot and $\Theta = (\theta_1 \dots \theta_{m-1})$ is a list of angles, where $\theta_i \in \mathcal{S}^1$ is the angle between the x -axis and link i . We omit here details regarding the metric in order to simplify the presentation. Clearly, a rigorous proof will have to take the specific metric into consideration.

We are now ready to state our claims. First, we show that given a point $q \in \mathbb{R}^2$, there is a configuration $C \in \mathcal{V}$, where $C = (p, \Theta)$, such that p and q are sufficiently close (in the Euclidean distance). This means that the robot’s head can achieve coverage of \mathbb{R}^2 , i.e., *head coverage*. We also require *angle coverage*: given a configuration $C_S = (q, \Theta_S) \in \mathcal{F}^S$, there exists $C = (p, \Theta) \in \mathcal{V}$ such that Θ and Θ_S are sufficiently close. Notice that the latter property easily follows from the fact that base configurations are uniformly sampled from \mathcal{F}^S . Combining the two coverage properties, we have a full coverage of \mathcal{F}^S .

We show the claim of head coverage using the following two steps.

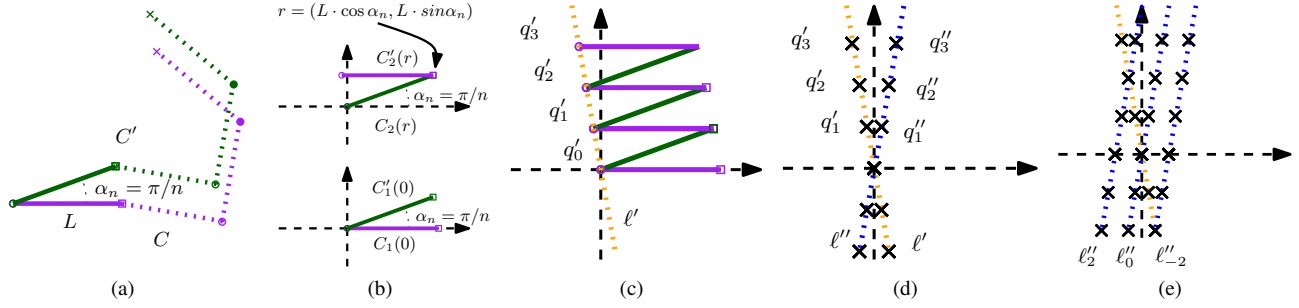


Fig. 5. Construction used head coverage. (a) Base configurations C (purple) and C' (green) which are identical except for the first angle $\alpha_n = \pi/n$. The first link (of length L) of the base configurations is depicted using solid lines and only it will be used in (b) and (c). (b) The two base roadmaps $G_1(\mathbf{0}), G_2(r)$ for C, C' . (c) Iteratively constructing the points $\{q'_i\}$ which densely lie on the line ℓ' passing through the origin. (d) The points $\{q''_i\}$ constructed using C, C'' (C'' is identical to C except for the first angle $-\alpha_n$). (e) The grid of points (black crosses) where the head of the robot may lie (step **S2**) induced by ℓ' (dashed yellow line) and parallel copies of ℓ'' (dashed blue line). Only every other copy of ℓ'' is depicted to avoid cluttering the figure.

S1 Given a start configuration where the head of the robot is at the origin $\mathbf{0}$, one can construct a straight line ℓ' in \mathbb{R}^2 such that (i) ℓ' intersects $\mathbf{0}$ and (ii) for every point on ℓ' , there exists a vertex in the tiling map whose head lies on ℓ' and is close to p up to any desired resolution as the number of samples tends to infinity.

S2 The construction in step **S1** can be used to construct two non-parallel lines ℓ', ℓ'' that span \mathbb{R}^2 . This in turn implies that ℓ', ℓ'' induce a grid such that any point in \mathbb{R}^2 is as close as desired to a grid point.

Sketch of step S1: Set $\alpha_n = \pi/n$ and assume that the following configurations are in the set of n base configurations: $C = (\mathbf{0}, 0, \theta_2 \dots \theta_{m-1})$ and $C' = (\mathbf{0}, \alpha_n, \theta_2 \dots \theta_{m-1})$. Namely, C is the base configuration where the head of the robot is placed at the origin, the first link lies on the x -axis and the remaining angles $\theta_2 \dots \theta_{m-1}$ are uniformly chosen. C' is defined in a similar manner, except that the first link has a small angle of α_n with the x -axis. See Fig. 5a. Moreover, we assume that C, C' are neighbors in both base roadmaps $G_1(\mathbf{0})$ and $G_2(\mathbf{0})$ (namely, the base roadmaps of the first two anchor points). Such an assumption is valid since both C, C' are self-collision free and there exists a self-collision free path between the two. Thus, we only assume that they are indeed nearest neighbors, which is true for sufficiently large value of k , which represents the maximal vertex degree in every base roadmap. See Fig. 5b.

We will show that using the assumption that C, C' are neighbors in both base roadmaps $G_1(\mathbf{0})$ and $G_2(\mathbf{0})$, we can construct a series of points $\{q'_i \mid i \in \mathbb{N}\}$ which lie on a line intersecting the origin. These points represent locations where the head of the robot may be reached by traversing \mathcal{G} (using exclusively the configurations C, C' and the base roadmaps $G_1(\mathbf{0}), G_2(\mathbf{0})$). Moreover, these points get arbitrarily close to one another as the number of samples grows (which causes α_n to decrease). The construction is fairly simple. Set $q'_0 = \mathbf{0}$, q'_1 is obtained by moving from $C_1(\mathbf{0})$ to $C'_1(\mathbf{0})$ in $G_1(\mathbf{0})$ and then shifting to the roadmap $G_2(r)$ (for the appropriate point $r = (L \cos \alpha_n, L \sin \alpha_n)$). This allows to move from $C'_2(r)$ to $C_2(r)$ in $G_2(r)$. Finally,

we set q'_1 to be the head of the robot in configuration $C_2(r)$. This process may be repeated from q'_1 to obtain q'_2 and henceforth. Fig. 5c provides a visualization of the construction of the points $\{q'_i \mid i \in \mathbb{N}\}$.

Recall that L represents the length of the first link. Using basic trigonometry we have that

$$q'_i = (i \cdot L(\cos \alpha_n - 1), i \cdot L \sin \alpha_n).$$

Moreover, all such points q'_i lie on a line ℓ' intersecting the origin and every two consecutive points are of (Euclidean) distance

$$\Delta(n) = \|q'_{i+1} - q'_i\|_2 = 2L \sin \frac{\alpha_n}{2} = 2L \sin \frac{\pi}{2n}.$$

Clearly $\lim_{n \rightarrow \infty} \Delta(n) = 0$.

Sketch of step S2: The construction of the line ℓ' in step **S1** was described for a specific pair of configurations C, C' . Now, if we consider the configuration $C'' = (\mathbf{0}, -\alpha_n, \theta_2 \dots \theta_{m-1})$, the same construction holds for the pair of configurations C, C'' to obtain the points $\{q''_i \mid i \in \mathbb{N}\}$ who all lie on the line ℓ'' and for which

$$q''_i = (i \cdot L(\cos \alpha_n - 1), -i \cdot L \sin \alpha_n).$$

Notice that ℓ' and ℓ'' are not parallel. Moreover, although the construction of ℓ' and ℓ'' was shown using the base roadmap $G_1(\mathbf{0})$, it holds for any point p where the head of the robot may be placed using the tiling roadmap. Specifically, one can construct the set of lines $\{\ell''_i \mid i \in \mathbb{N}\}$ which are parallel to ℓ'' such that for every $i \in \mathbb{N}$, ℓ''_i intersects ℓ' at the point q'_i . This induces a grid on the plane with growing resolution as the number of samples grows. See Fig. 5e.

B. On the probabilistic completeness of the tiling roadmap

We hope that the analysis presented for coverage will pave the way to a probabilistic completeness proof of our method. Typical proofs of probabilistic completeness (see, e.g., [43], [44]) rely on two properties of the examined algorithm. First, they require that the algorithm will provide *coverage* of the space. Secondly, every two close-by configurations need to be connected by an edge in the roadmap and the

corresponding local path should remain in the proximity of the connected configurations. In our case it is unclear whether the tiling roadmap abides by the second constraint.

VII. EVALUATION

We present simulation results evaluating the performance of our TR-dRRT framework on various scenarios and types of robots in a planar environment. We compare its running times with RRT [45] and RV-RRT [30]. Our C++ implementation follows the generic programming paradigm [46], which exploits the similarity between the behavior of the three algorithms in the query stage, and allows them to run on a mutual code framework. The only fundamental difference lies in the type of the extension method used. In particular, whereas RRT and RV-RRT employ a steering function, dRRT relies on an oracle that can efficiently query for neighbors in the *precomputed* tiling roadmap. We use the Euclidean metric for distance measurement and nearest-neighbor search. Specifically, every configuration is treated as a point in \mathbb{R}^{2m} , which represents the coordinates of the m anchor points. Nearest-neighbor search is performed using FLANN [47] and collision detection is done using a 2D adaptation of PQP [48]. All experiments were run on a laptop with 2.8GHz Intel Core i7 processor with 8GB of memory.

A. Test scenarios

We experimented with three types of multi-link robots in a planar environment with polygonal obstacles: free-flying open chains, free-flying closed chains, and anchored open chains.

The first type of robots requires primitive operations (sampling and local planning) that are straightforward to implement. For such cases, RRT is the most suitable algorithm to compare with TR-dRRT. Sample configurations for RRT and TR-dRRT were generated in a uniform fashion, and local planning was done by selecting one anchor point and performing interpolation between the angles of the joints, while maintaining the anchor point in a fixed position. The scenarios used to compare the two algorithms for the first type of robots are shown in Fig. 1a-1c. In the Tight scenario (Fig. 1a), a robot with nine links navigates in tight quarters among obstacles. The Coiled scenario (Fig. 1b) depicts a robot with ten links which needs to uncoil itself. This represents a scenario where the majority of the collisions that occur are self collision. In the Bricks scenario (Fig. 1c) a small 13-linked robot needs to move from a start configuration with little clearance to the goal. Note that the figure depicts a closed-chain robot as the same scenario is used for different robot types. The robot used in the open-chain case is identical to the closed chain, except that one of the links is removed.

The second type of robots are free-flying closed chains, which are significantly more complex to deal with, as the set of collision-free configurations lie on a low-dimensional manifold. RV-RRT [30] is arguably the most suitable algorithm for this type of robots. In these settings, TR-dRRT uses the primitive operations of RV-RRT for sampling and

local planning. We use a robot with 12 links and evaluate the two algorithms on the Tight (Fig 1a) and Bricks (Fig 1c) scenarios. For TR-dRRT the *same* preprocessed roadmap was used to answer the queries for the different scenarios, as we use the same robot (see Fig. 1).

The third type of robot is an open chain with one of its joints permanently anchored to a fixed point in the plane. Here we make a first step toward applying TR-dRRT to anchored robot arms. In the Gripper scenario (Fig.1d), a 10-link robot is anchored at its middle joint and both of the robot’s endpoints need to reach the goal region. This simulates two robotic arms that need to grasp an object. We constructed one base roadmap representing configurations where the middle joint is anchored. Currently, it is not clear how to extend the tiling-roadmap concept to the case of anchored robots (see discussion in Section VIII). Thus, we resort to dense sampling in the preprocessing stage. In the query stage, this roadmap was traversed using dRRT. We note that more suitable algorithms to solve this problem might exist. However, the simple approach described here, which outperforms RRT, serves as a proof of concept for the applicability of our technique to anchored-robot settings as well.

B. Experiments

We first study the affect that the number of sampled base configurations n has on the query time of TR-dRRT. We then proceed to compare the performance of TR-dRRT with RRT and RV-RRT.

TR-dRRT Preprocessing time. For each robot type, we gradually increased n . For each such value, we constructed the tiling roadmap with k nearest neighbors⁵ Finally, each roadmap was used to solve the aforementioned scenarios. Fig. 6 reports on the results for the open-chain nine-link robot used in the Tight scenario and the closed-chain robot used in the Bricks scenario. The reported preprocessing times are averaged over five different tiling roadmaps and the query times are averaged over 100 different queries, for each n . Not surprisingly, as n grows, the preprocessing times increase while the query times decrease: As the number of base configurations increases, each base roadmap captures more accurately the configuration space of the robot anchored to the respective joint. This leads to a better representation of \mathcal{F} using \mathcal{G} . Interestingly, for both cases reported, there exists a threshold for which the reduction of query times is insignificant and comes at the cost of exceedingly-large preprocessing times. Similar results were obtained for the other robot types.

Comparison with RRT and RV-RRT. In this set of experiments we compare the query time of TR-dRRT with RRT or RV-RRT for the aforementioned test scenarios. In these experiments TR-dRRT employs the most dense precomputed base roadmaps (see above). We mention that we

⁵We set $k = 2e \log n$ in order to reduce the number of parameters involved in the experiments. Such a number of neighbors can lead to asymptotic optimality of sampling-based motion-planning algorithms in certain situations (see, [5]), although we do not make such a claim here.

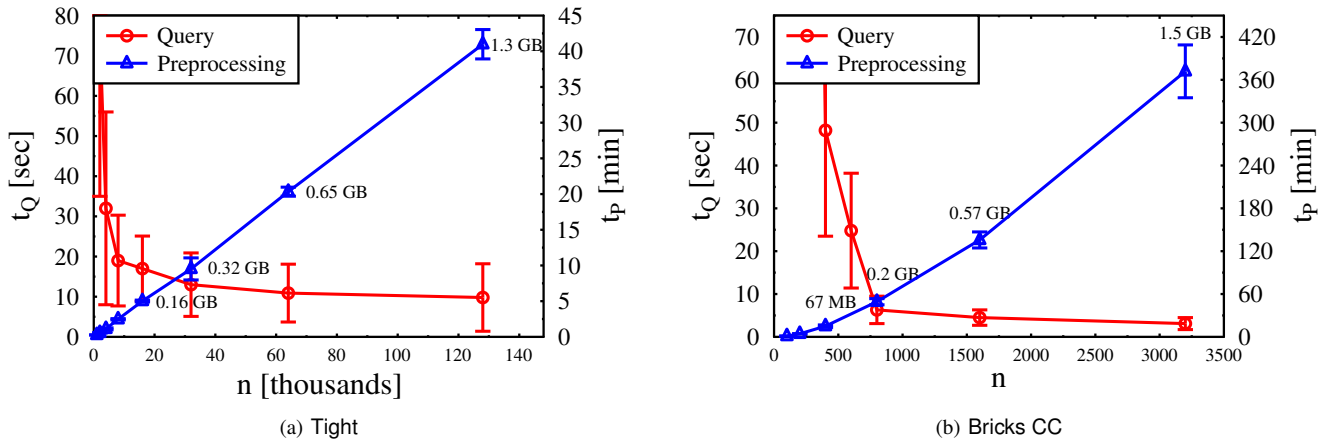


Fig. 6. Quality of results as a function of preprocessing times. Query time t_Q (left y-axis) and preprocessing time t_P (right y-axis) as a function of the number n of base configurations for the open-chain nine-link robot in the Tight scenario (a) and the closed chain robot used in the Bricks scenario (b). Error bars denote one standard deviation. Size of the tiling roadmap after preprocessing is added (only partial values are given to avoid cluttering the graph).

are not concerned with the quality of the solution, and only measure the time required to answer a query successfully. The preprocessing times for constructing the tiling roadmaps for the open-chain robots (Fig. 1-3) are fairly low (up to three minutes). For the Gripper scenario, we had to apply longer preprocessing times (roughly ten minutes) in order to construct a dense roadmap. For the closed-chain scenarios, preprocessing times were in the order of several hours. We note, however, that even fairly moderate preprocessing times could have obtained almost the same speedups (see Fig. 6). For the open-chain robots, both in the Tight and in the Coiled scenarios, TR-dRRT is roughly ten times faster than the RRT algorithm, while in the Bricks scenario, TR-dRRT is roughly five times faster than the RRT algorithm. For the Gripper scenario, TR-dRRT is roughly twice as fast as the RRT algorithm. In more complex problems with closed-chain robots TR-dRRT is roughly more than fifty times faster than RV-RRT, which is arguably the state-of-the-art for such problems.

VIII. DISCUSSION AND FUTURE WORK

This paper introduces a new paradigm in sampling-based motion-planning in which the specific structure of the robot is taken into consideration to reduce the amount of self-collision checks one has to perform online. We demonstrate this paradigm using the TR-dRRT algorithm which is designed for free-flying multi-link robots. TR-dRRT performs a preprocessing stage, which results in an implicit tiling roadmap that represents an infinite set of configurations and transitions which are entirely self-collision free. Given a query, the search of the configuration space is restricted to the tiling roadmap. As a result, no self-collision checks need to be performed, and the query stage is dedicated exclusively to finding an *obstacle*-collision free path.

We note that the preprocessing stage can be performed on stronger machinery, e.g., using cloud computing, than the

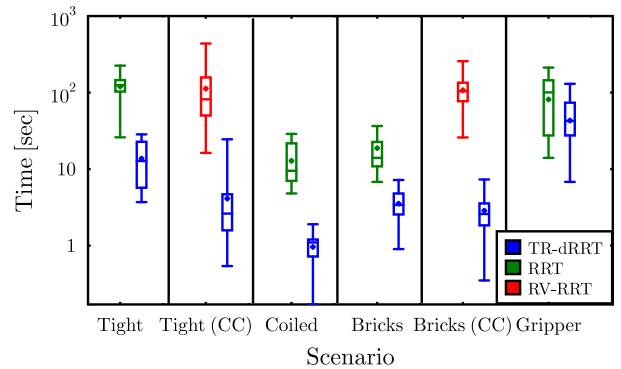


Fig. 7. Running times in seconds for the TR-dRRT (blue), RRT (green), and RV-RRT (red) algorithms (ten different runs), given as box plots: Lower and upper horizontal segments represent minimal and maximal running times, respectively; The diamond represents the average running time; The line in the middle of each box is the median, and the top and bottom of each box represent the 75th and 25th percentile, respectively. CC denotes that a closed-chain robot was used in the scenario. Notice that the time axis is in log scale.

one available to the robot in the query stage. Moreover, the preprocessing stage may easily be sped up by computing the individual base roadmaps in parallel.

To conclude, we point out an additional benefit of the TR-dRRT framework and suggest a direction for future research.

Reducing interpolation costs. Our framework can be used not only to eliminate self-collision checks, but also to reduce the cost of computing local plans (interpolations between two configurations) during the query stage. The cost of computing a local plan becomes significant when the number of degrees of freedom of the robot is high or when the robot has closed chains. As the base roadmaps specify which local plans can be used in the query stage, such plans can be precomputed and stored for every edge of the base roadmaps. Moreover, every local plan can be represented in

a structure that can reduce the running time of obstacle-collision checks. For instance, in our implementation we represent every local plan as a polygon that bounds the swept area⁶ of the respective motion. In particular, for every edge of a base roadmap (but not the tiling roadmap) we generate the swept area of the respective robot motion and generate a polygon which approximates the boundary of the swept area. This allows to perform a single obstacle-collision check for a given local plan, rather than densely sampling configurations along the motion and testing individually each and every configuration for collision. Specifically, whenever an edge of the tiling roadmap needs to be tested for obstacle collision during the query stage, the polygon which corresponds to the base-roadmap edge is extracted, translated according to the translation of the tiling roadmap edge, and tested for collision with the obstacles.

Recursive TR-dRRT. Although the experimental results are promising, TR-dRRT has its limitations. The explicitly-represented base roadmaps should accurately capture the self-collision free spaces for which one of the anchor points of the robot is fixed. For a robot with D degrees of freedom moving in \mathbb{R}^d , this space is $(D - d)$ -dimensional. Clearly, the favorable characteristics of our approach diminish as D increases. To overcome the so-called “curse of dimensionality” for this specific type of robots, we believe that one can apply our technique in a recursive manner. For instance, assume that the self-collision free space of a “snake-like” robot with $m - 1$ links (or m anchor points) can be captured by a roadmap accurately and efficiently. Now, given a robot with $2m - 2$ links, it can be decomposed into two parts, consisting of $m - 1$ links each. Then one can generate a tiling roadmap for each of the two parts and combine the two roadmaps into one, which, in turn, provides a covering of the entire self-collision free space. This bears resemblance to existing methods which recursively use copies of precomputed subspaces in motion-planning algorithms [49] or iteratively solve increasingly difficult relaxations of the given motion-planning problem [50], both of which have been shown as effective tools to enhance motion-planning algorithms.

REFERENCES

- [1] J. T. Schwartz and M. Sharir, “On the “piano movers” problem: II. General techniques for computing topological properties of real algebraic manifolds,” *Advances in Applied Mathematics*, vol. 4, no. 3, pp. 298–351, 1983.
- [2] J. H. Reif, “Complexity of the mover’s problem and generalizations (extended abstract),” in *FOCS*, 1979, pp. 421–427.
- [3] H. Choset, K. M. Lynch, S. Hutchinson, G. Kantor, W. Burgard, L. E. Kavraki, and S. Thrun, *Principles of robot motion: Theory, algorithms, and implementation, Chapter 7*. MIT Press, 2005.
- [4] S. M. LaValle, *Planning algorithms*. Cambridge University Press, 2006.
- [5] S. Karaman and E. Frazzoli, “Sampling-based algorithms for optimal motion planning,” *I. J. Rob. Res.*, vol. 30, no. 7, pp. 846–894, 2011.
- [6] K. Solovey, O. Salzman, and D. Halperin, “Finding a needle in an exponential haystack: discrete RRT for exploration of implicit roadmaps in multi-robot motion planning,” *I. J. Rob. Res.*, 2015, to appear.
- [7] L. E. Kavraki, P. Svestka, J. Latombe, and M. H. Overmars, “Probabilistic roadmaps for path planning in high-dimensional configuration spaces,” *T. Rob. and Aut.*, vol. 12, no. 4, pp. 566–580, 1996.
- [8] S. M. LaValle and J. J. Kuffner, “Randomized kinodynamic planning,” *I. J. Rob. Res.*, vol. 20, no. 5, pp. 378–400, 2001.
- [9] J. H. Yakey, S. M. LaValle, and L. E. Kavraki, “Randomized path planning for linkages with closed kinematic chains,” *T. Rob. and Aut.*, vol. 17, no. 6, pp. 951–958, 2001.
- [10] L. Han, “Hybrid probabilistic roadmap Monte Carlo motion planning for closed chain systems with spherical joints,” in *ICRA*, 2004, pp. 920–926.
- [11] L. Han and N. Amato, “A Kinematics-based probabilistic roadmap method for closed chain systems,” in *WAFR*, 2000, pp. 233–246.
- [12] J.-P. Merlet, “A local motion planner for closed-loop robots,” in *IROS*, 2007, pp. 3088–3093.
- [13] X. Tang, S. L. Thomas, P. Coleman, and N. M. Amato, “Reachable distance space: Efficient sampling-based planning for spatially constrained systems,” *I. J. Rob. Res.*, vol. 29, no. 7, pp. 916–934, 2010.
- [14] Y. Zhang, K. Hauser, and J. Luo, “Unbiased, scalable sampling of closed kinematic chains,” in *ICRA*, 2013, pp. 2459–2464.
- [15] L. Han, L. Rudolph, J. Blumenthal, and I. Valodzin, “Stratified deformation space and path planning for a planar closed chain with revolute joints,” in *WAFR*, 2006, pp. 235–250.
- [16] J. Cortés and T. Siméon, “Sampling-based motion planning under kinematic loop-closure constraints,” in *WAFR*, 2004, pp. 75–90.
- [17] F. Schwarzer, M. Saha, and J.-C. Latombe, “Adaptive dynamic collision checking for single and multiple articulated robots in complex environments,” *Robotics, Trans. on*, vol. 21, no. 3, pp. 338–353, 2005.
- [18] V. R. de Angulo, J. Cortés, and T. Siméon, “BioCD : An efficient algorithm for self-collision and distance computation between highly articulated molecular models,” in *RSS*, 2005, pp. 241–248.
- [19] I. Lotan, F. Schwarzer, D. Halperin, and J. Latombe, “Efficient maintenance and self-collision testing for kinematic chains,” in *SoCG*, 2002, pp. 43–52.
- [20] S. Redon, Y. J. Kim, M. C. Lin, and D. Manocha, “Fast continuous collision detection for articulated models,” in *Symposium on Solid Modeling and Applications*, 2004, pp. 145–156.
- [21] N. M. Amato and G. Song, “Using motion planning to study protein folding pathways,” *Journal of Computational Biology*, vol. 9, no. 2, pp. 149–168, 2002.
- [22] A. M. Ladd and L. E. Kavraki, “Using motion planning for knot untying,” *I. J. Rob. Res.*, vol. 23, no. 7-8, pp. 797–808, 2004.
- [23] B. Raveh, A. Enosh, O. Schueler-Furman, and D. Halperin, “Rapid sampling of molecular motions with prior information constraints,” *PLoS Computational Biology*, vol. 5, no. 2, 2009.
- [24] G. Song and N. M. Amato, “A motion-planning approach to folding: from paper craft to protein folding,” *T. Rob. and Aut.*, vol. 20, no. 1, pp. 60–71, 2004.
- [25] K. Kotay, D. Rus, M. Vona, and C. McGray, “The self-reconfiguring robotic molecule: Design and control algorithms,” in *WAFR*, 1998, pp. 375–386.
- [26] A. Nguyen, L. J. Guibas, and M. Yim, “Controlled module density helps reconfiguration planning,” in *WAFR*, 2000, pp. 15–27.
- [27] J. Latombe, “Motion planning: A journey of robots, molecules, digital actors, and other artifacts,” *I. J. Rob. Res.*, vol. 18, no. 11, pp. 1119–1128, 1999.
- [28] T. McMahan, S. L. Thomas, and N. M. Amato, “Sampling-based motion planning with reachable volumes: Theoretical foundations,” in *ICRA*, 2014, pp. 6514–6521.
- [29] —, “Sampling based motion planning with reachable volumes: Application to manipulators and closed chain systems,” in *IROS*, 2014, pp. 3705–3712.
- [30] —, “Reachable volume RRT,” in *ICRA*, 2015, pp. 2977–2984.
- [31] J. Pan, L. Zhang, and D. Manocha, “Retraction-based RRT planner for articulated models,” in *ICRA*, 2010, pp. 2529–2536.
- [32] R. Bohlin and L. E. Kavraki, “Path planning using lazy PRM,” in *ICRA*, 2000, pp. 521–528.
- [33] J. O’Hara, “The configuration space of a spider,” *Knots and Everything Book*, vol. 40, pp. 245–252, 2007.
- [34] N. Shvalb, M. Shoham, and D. Blanc, “Motion planning for a class of planar closed-chain manipulators,” *Forum Mathematicum*, vol. 17, no. 6, pp. 1033–1042, 2005.
- [35] G. Liu and J. C. Trinkle, “Complete path planning for planar closed chains among point obstacles,” in *RSS*, 2005, pp. 33–40.

⁶The swept area is the overall collection of points which the robot covers during a given motion.

- [36] J. C. Trinkle and R. J. Milgram, "Complete path planning for closed kinematic chains with spherical joints," *I. J. Rob. Res.*, vol. 21, no. 9, pp. 773–790, 2002.
- [37] N. Shvalb, M. Shoham, G. Liu, and J. C. Trinkle, "Motion planning for a class of planar closed-chain manipulators," *I. J. Rob. Res.*, vol. 26, no. 5, pp. 457–473, 2007.
- [38] J. M. Porta, J. Cortés, L. Ros, and F. Thomas, "A space decomposition method for path planning of loop linkages," in *IROS*, 2007, pp. 1882–1888.
- [39] J. M. Porta, L. Ros, and F. Thomas, "A linear relaxation technique for the position analysis of multiloop linkages," *Tran. on Rob.*, vol. 25, no. 2, pp. 225–239, 2009.
- [40] Z. Luo, Y. Chiang, J. Lien, and C. Yap, "Resolution-exact algorithms for link robots," in *WAFR*, 2014, pp. 353–370.
- [41] M. Likhachev, G. J. Gordon, and S. Thrun, "ARA*: Anytime A* with provable bounds on sub-optimality," in *Neural Information Processing Systems*, 2003, pp. 767–774.
- [42] J. Pearl, *Heuristics: Intelligent search strategies for computer problem solving*. Addison-Wesley, 1984.
- [43] L. E. Kavraki, M. N. Kolountzakis, and J. Latombe, "Analysis of probabilistic roadmaps for path planning," *T. Rob. and Aut.*, vol. 14, no. 1, pp. 166–171, 1998.
- [44] A. M. Ladd and L. E. Kavraki, "Generalizing the analysis of PRM," in *ICRA*, 2002, pp. 2120–2125.
- [45] J. Kuffner and S. LaValle, "RRT-connect: An efficient approach to single-query path planning," in *ICRA*, 2000, pp. 995–1001 vol.2.
- [46] M. H. Austern, *Generic programming and the STL: using and extending the C++ Standard Template Library*. Boston, MA, USA: Addison-Wesley Longman Publishing Co., Inc., 1998.
- [47] M. Muja and D. G. Lowe, "Fast approximate nearest neighbors with automatic algorithm configuration," in *VISSAPP*. INSTICC Press, 2009, pp. 331–340.
- [48] GAMMA group, "PQP - a proximity query package," 1999. [Online]. Available: <http://gamma.cs.unc.edu/SSV>
- [49] O. Salzman, M. Hemmer, and D. Halperin, "On the power of manifold samples in exploring configuration spaces and the dimensionality of narrow passages," *IEEE T. Automation Science and Engineering*, vol. 12, no. 2, pp. 529–538, 2015.
- [50] O. B. Bayazit, D. Xie, and N. M. Amato, "Iterative relaxation of constraints: a framework for improving automated motion planning," in *IROS*, 2005, pp. 3433–3440.